coatings

MDPI

Article

Synthesis of Nanoporous TiO_2 with the Use of Diluted Hydrogen Peroxide Solution and Its Application in Gas Sensing

Orhan Sisman *, Nicola Poli, Dario Zappa and Elisabetta Comini

Sensor Laboratory, Department of Information Engineering (DII), Università degli Studi di Brescia, Via Valotti 7, 25123 Brescia, Italy; nicola.poli@unibs.it (N.P.); dario.zappa@unibs.it (D.Z.); elisabetta.comini@unibs.it (E.C.)

* Correspondence: o.sisman@unibs.it; Tel.: +39-030-371-5873

Received: 5 September 2019; Accepted: 17 October 2019; Published: 19 October 2019

Abstract: The chemical routes of metal oxidation in presence of hydrogen peroxide solutions are tailor-made for the synthesis of biocompatible metal oxide surfaces with clean intermediate and end products, such as oxides, hydroxides, hydrogen and water. The hydrolysis of titanium in hydrogen peroxide solutions is particularly interesting for medical applications, forming micro- and nanoscale titania surfaces. In this paper, the content of the hydrolysis solution is revised, allowing the fabrication of gas sensor devices based on nanoporous titania. Nanopore and microcrack formations were discussed in detail by monitoring the structural changes on the thin film surface with field-emission scanning electron microscopy (FE-SEM). A stable rutile crystalline phase was detected by glancing incidence X-ray diffraction (GI-XRD) measurement after repetitive hydrothermal processes. Electrical conductance measurements were carried out at high temperatures (400–600 °C) under humid airflow (40% RH@20 °C) with the injection of various concentrations of a wide set of test compounds (C_2H_3N, CO, H_2, NO_2, C_2H_6O), to observe the sensing capabilities of the material. Furthermore, the humidity effects on the sensing properties toward H_2, CO, and C_2H_6O have been discussed.

Keywords: nanoporous titania; hydrothermal preparation; rutile phase; gas sensor; humidity effect

1. Introduction

Metal oxides (MOXs) have played a big role in the development of technologies in various industrial applications. The huge progress in nanofabrication methods has boosted their use by introducing various cost-effective and reliable synthesis routes, especially with bottom-up approaches [1]. Nanofabrication has not only exploited their surface properties, but also allowed them to be integrated in small and portable devices. Among these MOX nanostructures, intrinsically multi-functional ones have attracted much more attention than others. For instance, titanium dioxide (TiO_2) nanostructures are one of these extremely useful materials. Titanium dioxide nanostructures have found various applications, as photocatalysts [2], biosensors [3], optoelectronics [4] and many more [5–8]. In most cases, the synthesis method for these structures is the hydrothermal process, because it is a low-cost, low-temperature and environmentally friendly process [9]. In particular, the hydrolysis of Ti in alkaline solutions and the hydrations of Ti salts are common ways for the hydrothermal synthesis of TiO_2 nanostructures [10]. The availability of various alkaline solutions (NaOH, KOH, etc.) and Ti salts ($TiCl_4$, etc.) offers the possibility of obtaining TiO_2 nanostructures with various morphologies, exhibiting different crystalline structures and surface properties, making them perfect candidates for gas sensor applications. On the other hand, the single-step hydrolysis of Ti in hydrogen peroxide (H_2O_2) solution has been drawing attention, especially in biomedical applications, since having multi-step processes involving various chemicals always carries some contamination risks. Tengvall et al. have worked

extensively on the interaction between Ti and peroxide solutions for biomedical implants [11–16]. In other studies, nanostructured titania gels and their crystallization processes have been investigated according to the effects of the solvent [17,18], additional chemicals [19–21], and temperature [22]. Radtke et al. studied in detail the photocatalytic properties and the biocompatibility of titania and titania alloy surfaces synthesized by hydrogen peroxide solutions and its derivatives [23–26]. Wu and Qi reported the synthesis of titania nanorods with the help of precursors [27]. Recent studies have shown that it is possible to detect some organic molecules by using the photocatalytic properties of nanostructured titania, synthesized in hydrogen peroxide [28,29]. All these findings have revealed the possibility of fabricating biocompatible titania-based organic sensors in near future. In this study, conductometric gas sensor application has been presented as a pioneer example of the use of these biocompatible sensing surfaces. The amounts of hydrogen peroxide solution and the titanium film thickness have been optimized to fabricate nanoporous TiO_2 directly on the active area of the sensors. This optimization is essential for obtaining proper device integration, avoiding the transfer of the nanoporous layer, and thus increasing the mechanical stability of the devices.

The high electrical resistance of bare TiO_2 nanostructures has restricted their applications in the gas sensing field [30]. In some studies, the use of pure nitrogen or argon as carrier gases, instead of synthetic air, has been a practical solution to keep electrical resistance in a favorable range for the investigation of the sensing properties. On the contrary, high percentages of oxygen, which are normally present in air, increase the electrical resistance of bare titania nanostructures to very high values, which requires complex and accurate electronics [30–34]. These studies have definitely contributed in explaining the gas sensing properties of titania, and may also have found some interesting application areas, but it is essential to understand how these sensors work in real-life conditions for practical usage. In other studies, TiO_2 nano-heterostructured materials (by doping, surface modifications, etc.) have been attracting attention, since most of them have been successful in reducing their high intrinsic electrical resistance to feasible values for device integration [31,35–39]. Despite these developments, the gas sensing properties of bare TiO_2 nanostructures have not been studied properly for practical use, and there are still some missing parts that prevent real-life applications. Herein, we report the intrinsic sensing properties of nanoporous titania, which have been investigated by conductometric measurements at high temperatures (400–600 °C) in dry and humid (40% RH@20 °C) air flows towards a wide set of target compounds (C_2H_3N, CO, H_2, NO_2, C_2H_6O).

2. Materials and Methods

2.1. Synthesis of Nanoporous TiO_2

Polycrystalline alumina substrates (2 mm × 2 mm, 99% purity, Kyocera, Japan) were used for the deposition of Ti films and the fabrication of chemical sensing devices. Substrates were cleaned in an ultrasonic bath using acetone, ethanol and deionized water, for 5 min each one. Ti films of two different thicknesses (100 nm and 1 µm) were deposited on the substrates by RF magnetron sputtering (Kenotec, Italy). The depositions were carried out at 300 °C and a pressure of 6.6×10^{-3} mbar, with 75 W RF magnetron power (Ar plasma). The synthesis of the nanoporous surface was performed by soaking the samples into a 15 mL H_2O_2 solution, systematically diluted from 15% to 2% at 80 °C for 20 h in a home-made hydrothermal reactor. Oxidation processes on each sample were repeated three times to get totally bleached surfaces. The samples were finally annealed in a furnace, working at atmospheric pressure, at 450 °C for 4 h, to enhance their crystallization and stability. The experimental process is summarized in Table 1.

Table 1. Hydrothermal treatment process for each sample.

Samples	Hydrothermal Solution	Hydrothermal Temperature	Hydrothermal Time	Repeated Cycle	Calcination
Ti film 1 µm	15% H_2O_2 (aq)	80 °C	20 h	3	450 °C 4 h
Ti film 100 nm	2% H_2O_2 (aq)	80 °C	20 h	3	450 °C 4 h

2.2. Sample Characterization

The surface morphologies were examined using a FE-SEM (Leo 1525 Gemini model; Carl Zeiss AG, Oberkochen, Germany) connected to an energy dispersive X-ray spectrometer (EDX, Oxford, UK), operated in the potential range of 0–10 kV. The crystalline phase was identified by XRD measurements (Empyrean diffractometer, PANalytical, Netherlands) carried out using Cu-LFF tube (λ = 1.5406 Å) operated at 40 kV/40 mA. The incident angle in glancing angle mode was 1.5° and the spectra were recorded by using a proportional Xe detector in the range of 20°–50°.

2.3. Preparation and Testing of Gas Sensors

To perform the gas functional measurements, the samples were equipped with electrical contacts on the top of the titania layer, while heaters were deposited on the backside of the alumina substrates by magnetron sputtering technique. Firstly, TiW and Pt contact pads were deposited to increase the adhesion, at 75 W DC power (Ar plasma), 6.6 × 10^{-3} mbar working pressure at 300 °C for 3 min, respectively. Afterwards, Pt interdigitated transducers (IDT) were deposited under the same temperature, pressure and DC power conditions for 20 min (≈1 µm thickness). The same procedure was used for the deposition of the heating element on the backside of the samples.

The functional testing system is characterized by a climatic chamber (Angelantoni, Italy, model MTC 120), whose role is to keep the stainless-steel test chamber at a constant ambient temperature (20 °C). To control the working temperatures of the sensors, the heating element of each device is powered by Thurlbly Thandar PL330DP power supplies. A Dreschel bottle, placed in a thermostatic bath set at 25 °C, generates a saturated humid airflow, which is then mixed with synthetic dry air to achieve the desired level of relative humidity (RH). The measurements were carried out at a humidity level of 40% with a flow of 200 sccm. The devices were exposed to several injections of different concentrations of hydrogen (H_2), ethanol (C_2H_6O), carbon monoxide (CO), nitrogen dioxide (NO_2) and acetonitrile (C_2H_3N), at working temperatures between 400 to 600 °C. Each gas was kept flowing inside the chamber for 30 min and then, to recover the baseline, the airflow was restored for 60 min. A schematic configuration of experimental process and measurement set up is given in Figure 1.

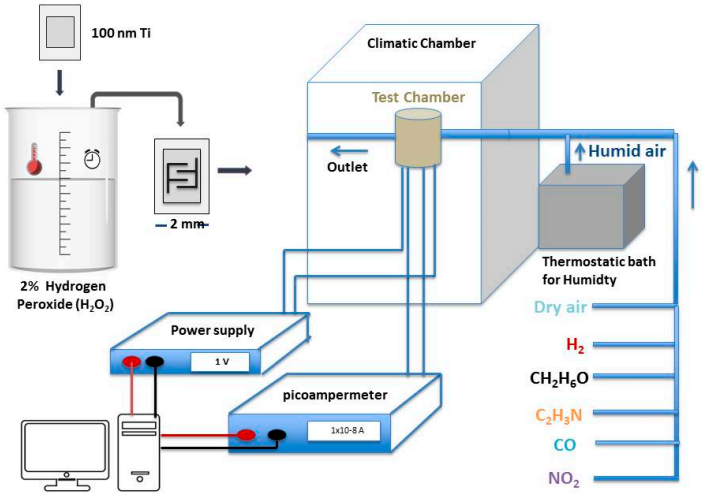

Figure 1. Schematic representation of experimental procedure and gas measurement system set up.

A voltage of 1 V was applied to the active layer using an Agilent E3631A power supply. The electrical conductance value of each device, crucial to determine the sensors response, was recorded by dedicated picoammeters (Keithley 486). The following equations (Equations (1) and (2))

highlight the relationship between the response of the sensors and the variations of the electrical conductance caused by the presence of oxidizing or reducing gas, respectively (for n-type):

$$\text{Response } (R) = \frac{G_{air} - G_{gas}}{G_{gas}} \text{ (for oxidizing gases)} \quad (1)$$

$$\text{Response } (R) = \frac{G_{gas} - G_{air}}{G_{air}} \text{ (for reducing gases)} \quad (2)$$

G_{air} and G_{gas} represent the conductance values of devices under synthetic airflow and in the presence of injected gas, respectively. Sensor response time (t_{res}) is defined as the time interval needed to reach a conductance value of 90% of $[G_{gas} - G_{air}]$ after the gas injection. Similarly, recovery time (t_{rec}) is the time interval needed to reach a conductance value reach of 90% of $[G_{gas} - G_{air}]$ after restoring the airflow. The calculations for R, $t_{res,}$ and t_{rec} were performed by an analysis program written according to the above equations and methods.

3. Results and Discussions

3.1. Characterization Results

Hydrogen peroxide (H_2O_2) solutions were diluted more than in previous studies in order to protect the structural integrity of the Ti thin films [40]. A dense and homogeneous formation of nanoporous TiO_2 was observed on the surface of the samples prepared using a 1 µm Ti thin film in 15% H_2O_2 solution, as reported in Figure 2a. Similar results were obtained using a 100 nm Ti thin film in 2% H_2O_2 solution, as reported in Figure 2b. Micro-cracks on the surface were observed in thicker thin films with higher peroxide concentrations. The use of thinner films and a lower concentration of hydrogen peroxide solution seemed to be effective on reducing the size of the cracks. Moreover, more dollops were attained on the surface with higher concentrations and thicker Ti films, as shown in Figure 2a. Therefore, nanoporous TiO_2 layers synthesized by the oxidation of 100 nm Ti thin films in 2% H_2O_2 solution were selected as the optimal morphology for gas sensor devices. The hydrothermal process was repeated three times (20 h each) until the nanoporous TiO_2 films were totally bleached. Sun and Wang described the possible chemical reactions (Equations (3)–(8)) that could occur during H_2O_2 oxidation [40]. Those reactions are reported below:

$$Ti + H_2O_2 \rightarrow TiO_2 + H_2 \quad (3)$$

$$2H_2O_2 \rightarrow 2H_2O + O_2 \quad (4)$$

$$TiO_2 + 2H_2O \rightarrow Ti(OH)_4 \quad (5)$$

$$TiO_2 + nH_2O \rightarrow TiO_2nH_2O \quad (6)$$

$$(Ti - OH) + H_2O \rightarrow [Ti - O]^- + H_3O^+ \quad (7)$$

$$TiO_2nH_2O + OH^- \rightarrow HTiO_3^-nH_2O \quad (8)$$

At low temperature, Ti reacts with hydrogen peroxide, forming titania phases (Equation (3)). At higher temperatures, some TiO_2 is hydrolyzed due to the effects of hot water and H_2O_2 (Equations (4)–(5)). Hydration reaction with TiO_2 takes place simultaneously, forming Ti–OH functional groups (Equation (6)). Hydrated and hydrolyzed TiO_2 cause the formation of negatively charged surfaces (Equations (7)–(8)), which are involved in the formation of nanoporous structures.

In addition to morphological analysis, EDX measurements were carried out on the samples to determine elemental composition and to detect possible contaminants. Figure 3 displays the quantitative elemental analysis results and the dispersion field of prepared samples using a 2% H_2O_2 solution. The inset table (Figure 3) gives the atomic percentages of existing elements. The rest of atomic

content (5.92%) belongs to carbon, which originated from natural carbon contamination and from carbon tape used to mount the substrate on the holder. Carbon was not shown in EDX analysis in order to prevent misunderstandings. Oxygen, aluminum, and titanium peaks are consistent with titania (TiO_2) and alumina (Al_2O_3) presence. The high amount of O (83.16%) could be linked to hydroxide (OH) species on the surface (Equations (7) and (8)).

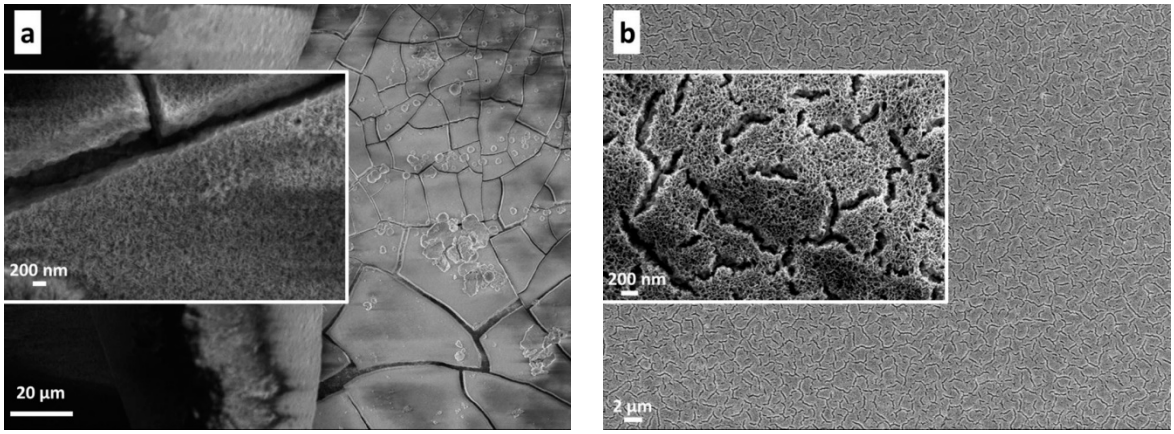

Figure 2. FE-SEM images of nanoporous TiO_2 surface (**a**) synthesized with oxidation of 1 µm Ti thin film in 15% H_2O_2 solution, (**b**) with oxidation of 100 nm Ti thin film in 2% H_2O_2 solution.

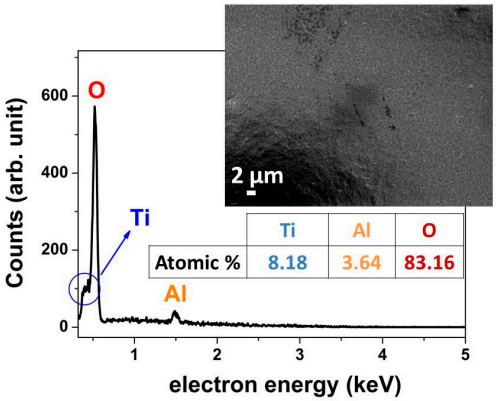

Figure 3. Energy dispersive of X-Ray spectrum of the nanoporous TiO_2 layer, synthesized in 2% H_2O_2 solution.

The crystalline structure of the synthesized nanoporous TiO_2 layer was determined by GI-XRD measurement. There are two overlapping measurement profiles in Figure 4, which belong to a wet oxidation sample before and after a thermal annealing in the furnace. In addition to alumina substrate peaks (+), the main characteristic peaks of TiO_2 rutile phase (*R*) belong to (110) plane, visible at 27.3°, as well as other rutile crystalline planes (101), (111) visible at 36° and 41.3° (JCPDS 21-1276). No peaks belonging to other phases were detected. Overlapping spectral peaks prove the stability of rutile-TiO_2 after the thermal process. In the literature, single rutile [27], single anatase [40], or dual rutile and anatase [41] phases were observed in samples fabricated by using similar solutions. Moreover, Wu observed single anatase or dual-phase in titania films when using a 30% H_2O_2 solution made by the oxidation of Ti powder and plates [21]. It was proposed that low Ti(IV) ion concentrations in the solution and an acidic environment (low pH value) could boost rutile phase formation [27,41,42]. In the present case, hydrogen peroxide has a weak acidity characteristic, so a natural growth of rutile phase could be derived with low degree of supersaturation because of small amount of H_2O_2 (2%) concentration and Ti thin film layer (100 nm) [41].

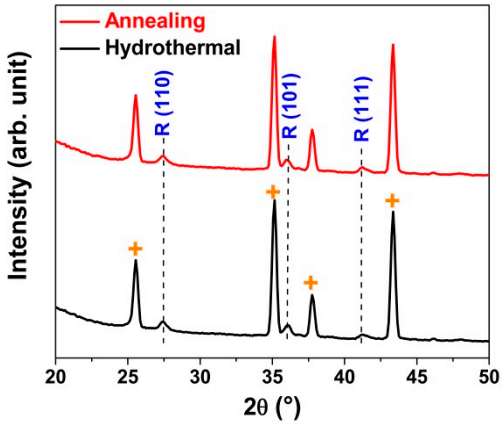

Figure 4. GI-XRD patterns of synthesized nanoporous TiO_2 film and after annealing, red and black spectra are almost overlapping.

3.2. Gas Sensing

The isothermal dynamic responses of the nanoporous TiO_2 layer towards hydrogen gas injections demonstrate the n-type semiconducting behavior of the material (Figure 5a). A visualization of the response and recovery times is presented in Figure 5b with the zoomed conduction curve of titania at 600 °C towards 500 ppm H_2. The electrical conductance increases upon interaction with reducing hydrogen gas. Due to the increased temperature, the oxygen molecules are dissociated and adsorbed on the titania surface in different forms (Equations (9) and (10)), depending on the sample temperature. For example, in the temperature range of 400–600 °C there are two different possible adsorption phases of oxygen ions [43]:

$$O_{2(g)} + 2e^- \leftrightarrow 2O^-_{(ads)} \quad (9)$$

$$O^-_{(ads)} + e^- \leftrightarrow O^{2-}_{(ads)} \quad (10)$$

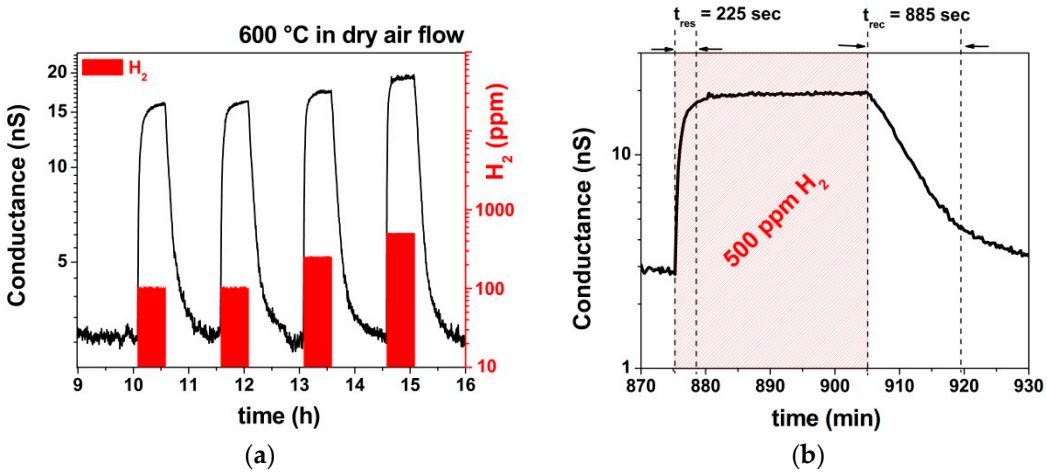

Figure 5. (**a**) Isothermal dynamic responses of nanoporous TiO_2 towards 100 ppm, 250 ppm, and 500 ppm H_2 gas at 600 °C. (**b**) Response and recovery curves towards 500 ppm H_2 injection.

The trapped electrons are released with the interaction of the reducing gas with chemisorbed oxygen ions. The possible reactions (Equations (11)–(15)) for reducing H_2 [44], C_2H_6O [45,46], C_2H_3N [47,48], CO [49] gases and oxidizing NO_2 [31] are given by the following equations:

$$H_{2(g)} + O^-_{(ads)} \leftrightarrow H_2O_{(g)} + e^- \quad (11)$$

$$CH_3CH_2OH_{(g)} + 6O^-_{(ads)} \leftrightarrow 2CO_{2(g)} + 3H_2O_{(g)} + 6e^- \quad (12)$$

$$CO_{(g)} + O^-_{(ads)} \leftrightarrow CO_{2(g)} + e^- \quad (13)$$

$$CH_3CN_{(g)} + 3O^-_{(ads)} \leftrightarrow CN^- + xCO + xCO_{2(g)} + (x+1)H_2O_{(g)} + 2e^- \quad (14)$$

$$NO_{2(g)} + e^- \leftrightarrow NO_{(g)} + O^-(ads) \quad (15)$$

Nanoporous TiO_2 gas sensors were tested towards C_2H_3N, CO, H_2, NO_2, and C_2H_6O in humid air (40% RH) flows. A comparison of the sensor responses towards fixed concentrations of target gases with working temperatures in the range 400–600 °C is given in Figure 6a. Sensors do not exhibit any appreciable response (≤0.1) in the presence of 10 ppm NO_2. It is worth reporting that there are no significant conductance changes in dynamic gas measurements towards 2 and 5 ppm NO_2 injections. Rutile phase may be responsible for NO_2 deafness since the crystalline phase of TiO_2 can be decisive for the detection of oxidizing gases as previously reported in literature [31,50]. Also, high working temperatures (>250 °C) are not favorable for NO_2 detection. The reducing gases (C_2H_3N, CO, H_2, and C_2H_6O) show similar trends: a small decrease in the response values at 450 °C followed by an increasing response up to 600 °C. On the other hand, there is a drastic decrease in NO_2 response value at 450 °C. It is plausible that not only temperature, but also humidity should be taken into consideration to explain these changes. However, due to the complexity of the involved surface chemical reactions, more in-depth investigations are required to fully understand the roles of humidity and temperature and how they affect the sensing properties. In operando measurements, for example, could provide useful information to better understand the surface chemistry.

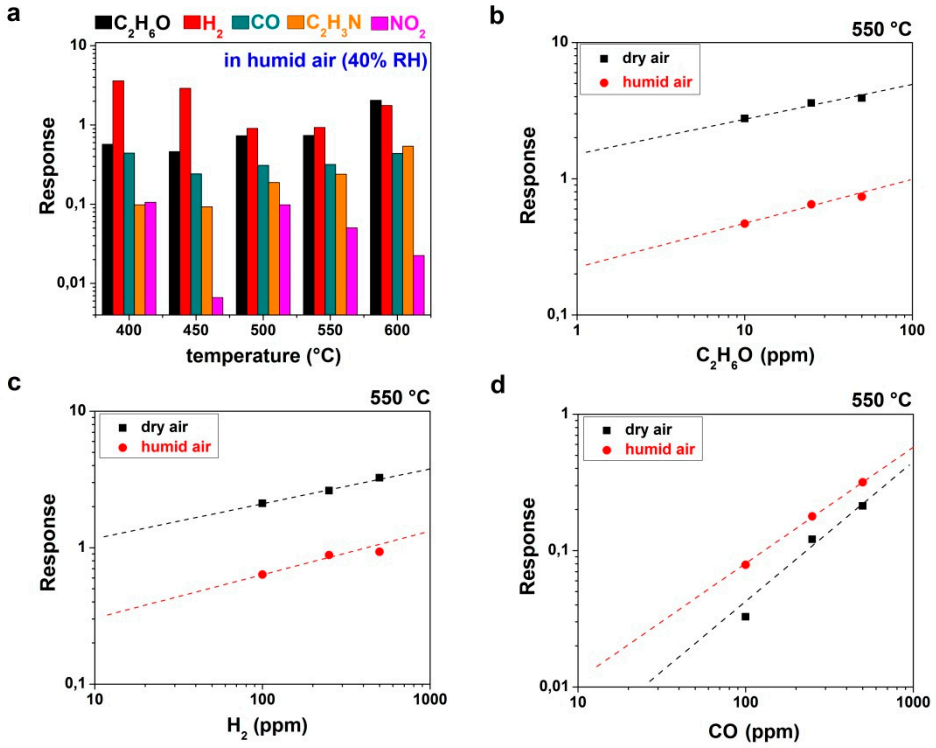

Figure 6. (**a**) Comparison of sensor responses at elevated working temperatures towards 50 ppm C_2H_6O, 500 ppm H_2, 500 ppm CO, 25 ppm C_2H_3N, 10 ppm NO_2 gases in humid air (40% RH) atmospheres. Logarithmic response values vs selected concentrations of (**b**) ethanol, (**c**) hydrogen, and (**d**) carbon monoxide.

Figure 6b–d presents more information about the effect of humidity on the sensing of H_2, C_2H_6O, and CO gases, by comparing the response in dry and humid air flows at 550 °C. There is a decrease of almost one order of magnitude in the response values for C_2H_6O and H_2 when introducing a humid airflow, while there is a small increase in response values for CO. These results again show that the interaction depends strongly on the chemical species involved. On a different semiconducting oxide (SnO_2), Barsan and Ionescu proposed that water molecules dissociate in H^+ and OH^-, which are absorbed on SnO_2 surface as hydroxyl group [51]. The participation of water vapor increases the interaction between atmospheric oxygen and n-type semiconductor surface, acting like a catalyst for this reducing gas [51]. This may also hold for TiO_2, and may explain the increase in the response value in presence of CO, since nanoporous TiO_2 shows a similar n-type behavior. In addition, the shorter response and recovery times in humid air for all reducing gases prove the existence of a catalytic effect for nanoporous TiO_2. On the other hand, the effect of water vapor seems to work in an opposite way for H_2 and C_2H_6O gases. The humidity reduced the sensor responses of H_2 and C_2H_6O. In contradiction with our observations, Moon et al. presented that H_2 sensing of mesoporous titania was not effected by humidity variations (5%, 15%, 42%RH) at 140 °C [52]. Similarly, hydrothermally grown TiO_2 nanorods did not change the response values towards 1–100 ppm VOCs (ethanol, methanol, and propanol) at 75 °C under humidity variations (8%, 52%, 75%RH) [53]. The most probable reason for both of these cases is that the working temperatures were too low to initialize a strong chemisorption of water molecules on the surface of TiO_2. The physisorption of water molecules has no effect on conduction [51]. In our case, the temperature was high enough for the chemisorption of water vapor on nanoporous titania surface. In addition to this, the hydrogen sensing mechanisms of titania surfaces were attributed mostly to spill-over effect [54,55]. Hydroxyl groups on the surface may behave as an anti-catalyst for dissociation and diffusion process of H_2 molecules, which is different from the adsorption of CO molecules. Ethanol sensing seems more complex because of its intermediate products during decomposition [56,57]. The authors indicate that similar observations for SnO_2 nanobelts were discussed and reported in a previous work [58]. The catalytic and anti-catalytic properties of hydroxyl groups might be effective for these dehydration (Equation (16)) and dehydrogenation (Equation (17)) reactions.

$$CH_3CH_2OH \rightarrow C_2H_4 + H_2O \quad (16)$$

$$CH_3CH_2OH \rightarrow CH_3CHO + H_2 \quad (17)$$

Table 2 summarizes the sensing performances of this work compared to some recent studies on bare-TiO_2 nanostructures, with numerical parameters. Some studies defined the sensor response value as the ratio of the electrical resistance value in air with the resistance value in the test gas (R_{air}/R_{gas}). These are indicated in parentheses next to their response values in the table. Our rutile nanoporous titania sensor had better response values towards H_2 and C_2H_6O than similar nanoporous TiO_2 sensors [38,52,59], as well as most other nanostructures [53,60–62]. Sensor response towards 25 ppm of C_2H_3N was 0.53 at 600 °C, which is an appropriate response value (≥0.1) to be used as an early detection system for acetonitrile exposure. Acetonitrile has toxic effects on the human body, and its odor threshold value is 42 ppm [63]. On the other hand, t_{res} and t_{rec} were longer than those reported in existing studies regarding H_2 and C_2H_6O gases. Higher working temperature and lower gas concentration values could be the reason for these long times. In general, high working temperatures are not preferable for smart gas sensor applications due to energy considerations. Nevertheless, high working temperatures are a natural requirement for bare semiconducting MOXs. Thanks to our synthesis method, which allows the easy fabrication of TiO_2 nanoporous sensing layers on 2 mm × 2 mm surface area, our sensors need only 0.5 W electrical power to work at 400 °C. Unfortunately, there are no available data to compare energy efficiency, although other similar nanoporous sensors have lower working temperature [52].

Table 2. Sensing performances of previously reported bare-TiO_2 nanostructure-based gas sensors in comparison with the present work.

Materials	Carrier Gas	Temp. (°C)	Target Gas	Response	Gas Conc. (ppm)	t_{res}/t_{rec} (sec/sec)	Ref.
NPorous TiO_2	Dry air	550	H_2	3.24	500	510/1155	This work
			C_2H_6O	3.90	50	1050/1830	
			CO	0.21	500	555/810	
	RH 40%	400	H_2	3.60	500	120/285	
			NO_2	0.1	10	t_{res} < 15/120	
		600	C_2H_6O	2.06	50	330/900	
			CO	0.43	500	405/255	
			C_2H_3N	0.53	25	270/450	
MPorous TiO_2	Dry air	140	H_2	2.8(R_{air}/R_{gas})	1000	5/125	[52]
	RH 42%	140	H_2	1.9(R_{air}/R_{gas})	100	~5/125	
NPorous TiO_2	Dry air	370	C_2H_6O	20(R_{air}/R_{gas})	1500	-	[38]
NPorous TiO_2	Dry air	225	H_2	1.2(R_{air}/R_{gas})	1%	-	[59]
TiO_2 NTubes	RH 40%	200	H_2	~10	1000	-	[35]
			C_2H_6O	~40	500	-	
			CO	~2	500	-	
			NO_2	~8	10	-	
TiO_2 NTubes	Dry air	200	C_2H_6O	2.9	5000	-	[60]
TiO_2 NRods	Dry air	75	C_2H_6O	0.69	100	13/23	[53]
	RH 52%	75	C_2H_6O	0.67	100	-	
TiO_2 NRods	Dry air	150	C_2H_6O	2.4(R_{air}/R_{gas})	25	55/80	[61]
TiO_2 Film	Dry air	RT	H_2	0.8	5000	~100/~10	[62]

4. Conclusions

The hydrolysis process of titanium thin film in peroxide solution was optimized for fabrication of nanoporous TiO_2 gas sensors. The 2% hydrogen peroxide solution was determined to be an optimal solution for nanoporous layer formation on 100 nm titanium thin film. The formation kinetics of nanoporosity were discussed and demonstrated with chemical reactions. The lower hydrogen peroxide concentration offers better mechanical strength for the sensor surface. The reduction in surface cracks and the decrease in the formation of dollops through the titania surfaces were monitored using FE-SEM images. In addition, one of the main motivations for this study was to use a clean synthesis method to protect the biocompatibility of TiO_2 surface. The EDX profile of the nanoporous surface proved the purity of the synthesis process. The rutile crystal structure and its thermal stability were screened by GI-XRD measurements of TiO_2 nanoporous samples before and after thermal annealing. After device configuration, high-temperature sensor tests were conducted in humid airflow with respect to different concentrations of H_2, C_2H_6O, CO, NO_2, and C_2H_3N. Our sensor reported better sensor response towards H_2 and C_2H_6O than similar nanoporous surfaces. The kinetics of chemical sensing was illustrated with reaction formulations for each gas. The catalytic and anti-catalytic effects of humidity were discussed in detail for reducing gases (H_2, C_2H_6O, CO) with their response value comparisons in dry and humid air flows.

Author Contributions: Conceptualization, E.C.; Data curation, O.S.; Funding acquisition, E.C.; Investigation, O.S. and N.P.; Methodology, O.S., N.P. and E.C.; Project administration, E.C.; Supervision, E.C.; Validation, O.S. and D.Z.; Writing—original draft, O.S.; Writing—review and editing, D.Z. and E.C.

Funding: This research received no external funding.

Acknowledgments: We would like to thank Angela Bertuna for her technical support in the preliminary activities of this study.

Conflicts of Interest: The authors declare no conflict of interest.

References

1. Devan, R.S.; Patil, R.A.; Lin, J.H.; Ma, Y.R. One-dimensional metal-oxide nanostructures: Recent developments in synthesis, characterization, and applications. *Adv. Funct. Mater.* **2012**, *22*, 3326–3370. [CrossRef]
2. Gao, R.; Jiao, Z.; Wang, Y.; Xu, L.; Xia, S.; Zhang, H. Eco-friendly synthesis of rutile TiO_2 nanostructures with controlled morphology for efficient lithium-ion batteries. *Chem. Eng. J.* **2016**, *304*, 156–164. [CrossRef]

3. Kulkarni, M.; Mazare, A.; Gongadze, E.; Perutkova, Š.; Kralj-Iglic, V.; Milošev, I.; Schmuki, P.; Iglič, A.; Mozetič, M. Titanium nanostructures for biomedical applications. *Nanotechnology* **2015**, *26*. [CrossRef] [PubMed]
4. Tian, W.; Lu, H.; Li, L. Nanoscale ultraviolet photodetectors based on onedimensional metal oxide nanostructures. *Nano Res.* **2015**, *8*, 382–405. [CrossRef]
5. Chen, B.; Hou, J.; Lu, K. Formation mechanism of TiO_2 nanotubes and their applications in photoelectrochemical water splitting and supercapacitors. *Langmuir* **2013**, *29*, 5911–5919. [CrossRef]
6. Li, H.; Chen, Z.; Tsang, C.K.; Li, Z.; Ran, X.; Lee, C.; Nie, B.; Zheng, L.; Hung, T.; Lu, J.; et al. Electrochemical doping of anatase TiO_2 in organic electrolytes for high-performance supercapacitors and photocatalysts. *J. Mater. Chem. A* **2014**, *2*, 229–236. [CrossRef]
7. Özgür, M.E.; Balcıoğlu, S.; Ulu, A.; Özcan, İ.; Okumuş, F.; Köytepe, S.; Ateş, B. The in vitro toxicity analysis of titanium dioxide (TiO_2) nanoparticles on kinematics and biochemical quality of rainbow trout sperm cells. *Environ. Toxicol. Pharmacol.* **2018**, *62*, 11–19. [CrossRef]
8. Leong, H.J.; Oh, S. Journal of Industrial and Engineering Chemistry Preparation of antibacterial TiO_2 particles by hybridization with azelaic acid for applications in cosmetics. *J. Ind. Eng. Chem.* **2018**, *66*, 242–247. [CrossRef]
9. Ge, M.; Cao, C.; Huang, J.; Li, S.; Chen, Z.; Zhang, K.-Q.; Al-Deyab, S.S.; Lai, Y. A review of one-dimensional TiO_2 nanostructured materials for environmental and energy applications. *J. Mater. Chem. A* **2016**, *4*, 6772–6801. [CrossRef]
10. Bavykin, D.V.; Friedrich, J.M.; Walsh, F.C. Protonated titanates and TiO_2nanostructured materials: Synthesis, properties, and applications. *Adv. Mater.* **2006**, *18*, 2807–2824. [CrossRef]
11. Tengvall, P.; Elwing, H.; Lundström, I. Titanium gel made from metallic titanium and hydrogen peroxide. *J. Colloid Interface Sci.* **1989**, *130*, 405–413. [CrossRef]
12. Tengvall, P.; Lundström, I.; Sjöqvist, L.; Elwing, H.; Bjursten, L.M. Titanium-hydrogen peroxide interaction: Model studies of the influence of the inflammatory response on titanium implants. *Biomaterials* **1989**, *10*, 166–175. [CrossRef]
13. Tengvall, P.; Bertilsson, L.; Liedberg, B.; Elwing, H.; Lundström, I. Degradation of dried Ti-peroxy gels made from metallic titanium and hydrogen peroxide. *J. Colloid Interface Sci.* **1990**, *139*, 575–580. [CrossRef]
14. Tengvall, P.; Hornsten, E.G.; Elwing, H.; Lundstrom, I. Bactericidal properties of a titanium-peroxy gel obtained from metallic titanium and hydrogen peroxide. *J. Biomed. Mater. Res.* **1990**, *24*, 319–330. [CrossRef]
15. Tengvall, P.; Wälivaara, B.; Westerling, J.; Lundström, I. Stable titanium superoxide radicals in aqueous Ti-peroxy gels and Ti-peroxide solutions. *J. Colloid Interface Sci.* **1991**, *143*, 589–592. [CrossRef]
16. Tengvall, P.; Vikinge, T.P.; Lundström, I.; Liedberg, B. FT-Raman Spectroscopic Studies of the Degradation of Titanium Peroxy Gels Made from Metallic Titanium and Hydrogen Peroxide. *J. Colloid Interface Sci.* **1993**, *160*, 10–15. [CrossRef]
17. Ayers, M.R.; Hunt, A.J. Titanium oxide aerogels prepared from titanium metal and hydrogen peroxide. *Mater. Lett.* **1998**, *34*, 290–293. [CrossRef]
18. Song, K.C.; Pratsinis, S.E. The effect of alcohol solvents on the porosity and phase composition of Titania. *J. Colloid Interface Sci.* **2000**, *231*, 289–298. [CrossRef]
19. Wang, X.-X.; Hayakawa, S. Improvement of bioactivity of H_2O_2/$TaCl_5$-treated titanium after subsequent heat treatments. *J. Biomed. Mater. Res.* **2000**, *52*, 171–176. [CrossRef]
20. Wu, J.M.; Hayakawa, S.; Tsuru, K.; Osaka, A. Nanocrystalline Titania Made from Interactions of Ti with Hydrogen Peroxide Solutions Containing Tantalum Chloride. *Cryst. Growth Des.* **2002**, *2*, 147–149. [CrossRef]
21. Wu, J.M. Low-temperature preparation of titania nanorods through direct oxidation of titanium with hydrogen peroxide. *J. Cryst. Growth* **2004**, *269*, 347–355. [CrossRef]
22. Wu, J.-M. Photodegradation of Rhodamine B in Water Assisted by Titania Nanorod Thin Films Subjected to Various Thermal Treatments. *Environ. Sci. Technol.* **2007**, *41*, 1723–1728. [CrossRef] [PubMed]
23. Radtke, A.; Piszczek, P.; Topolski, A.; Lewandowska, Z.; Talik, E.; Andersen, I.H.; Nielsen, L.P.; Heikkilä, M.; Leskelä, M. The structure and the photocatalytic activity of titania based nanotube and nanofiber coatings. *Appl. Surf. Sci.* **2016**, *368*, 165–172. [CrossRef]
24. Radtke, A.; Topolski, A.; Jędrzejewski, T.; Kozak, W.; Sadowska, B.; Więckowska-Szakiel, M.; Piszczek, P. Bioactivity studies on titania coatings and the estimation of their usefulness in the modification of implant surfaces. *Nanomaterials* **2017**, *7*, 90. [CrossRef]

25. Radtke, A.; Topolski, A.; Jędrzejewski, T.; Kozak, W.; Sadowska, B.; Więckowska-Szakiel, M.; Szubka, M.; Talik, E.; Nielsen, L.P.; Piszczek, P. The bioactivity and photocatalytic properties of titania nanotube coatings produced with the use of the low-potential anodization of Ti6Al4V alloy surface. *Nanomaterials* **2017**, *7*, 197. [CrossRef]
26. Radtke, A.; Bal, M.; Jędrzejewski, T. Novel titania nanocoatings produced by anodic oxidation with the use of cyclically changing potential: Their photocatalytic activity and biocompatibility. *Nanomaterials* **2018**, *8*, 712. [CrossRef]
27. Wu, J.M.; Qi, B. Low-temperature growth of monolayer rutile TiO_2 nanorod films. *J. Am. Ceram. Soc.* **2007**, *90*, 657–660. [CrossRef]
28. Mu, Q.; Li, Y.; Zhang, Q.; Wang, H. Template-free formation of vertically oriented TiO_2nanorods with uniform distribution for organics-sensing application. *J. Hazard. Mater.* **2011**, *188*, 363–368. [CrossRef]
29. Unosson, E.; Welch, K.; Persson, C.; Engqvist, H. Stability and prospect of UV/H_2O_2 activated titania films for biomedical use. *Appl. Surf. Sci.* **2013**, *285*, 317–323. [CrossRef]
30. Bayata, F.; Saruhan-Brings, B.; Ürgen, M. Hydrogen gas sensing properties of nanoporous Al-doped titania. *Sens. Actuators B Chem.* **2014**, *204*, 109–118. [CrossRef]
31. Gönüllü, Y.; Haidry, A.A.; Saruhan, B. Nanotubular Cr-doped TiO_2 for use as high-temperature NO_2 gas sensor. *Sens. Actuators B Chem.* **2015**, *217*, 78–87. [CrossRef]
32. Paulose, M.; Varghese, O.K.; Mor, G.K.; Grimes, C.A.; Ong, K.G. Unprecedented ultra-high hydrogen gas sensitivity in undoped titania nanotubes. *Nanotechnology* **2006**, *17*, 398–402. [CrossRef]
33. Lu, C.; Chen, Z. High-temperature resistive hydrogen sensor based on thin nanoporous rutile TiO_2film on anodic aluminum oxide. *Sens. Actuators B Chem.* **2009**, *140*, 109–115. [CrossRef]
34. Peng, X.; Wang, Z.; Huang, P.; Chen, X.; Fu, X.; Dai, W. Comparative study of two different TiO_2 film sensors on response to H_2 under UV light and room temperature. *Sensors* **2016**, *16*, 1249. [CrossRef]
35. Galstyan, V.; Comini, E.; Faglia, G.; Vomiero, A.; Borgese, L.; Bontempi, E.; Sberveglieri, G. Fabrication and investigation of gas sensing properties of Nb-doped TiO_2nanotubular arrays. *Nanotechnology* **2012**, *23*. [CrossRef]
36. Li, Z.; Ding, D.; Liu, Q.; Ning, C.; Wang, X. Ni-doped TiO_2 nanotubes for wide-range hydrogen sensing. *Nanoscale Res Lett.* **2014**, *9*, 118. [CrossRef]
37. Galstyan, V.; Comini, E.; Baratto, C.; Ponzoni, A.; Ferroni, M.; Poli, N.; Bontempi, E.; Brisotto, M.; Faglia, G.; Sberveglieri, G. Large surface area biphase titania for chemical sensing. *Sens. Actuators B Chem.* **2015**, *209*, 1091–1096. [CrossRef]
38. Chen, N.; Li, Y.; Deng, D.; Liu, X.; Xing, X.; Xiao, X.; Wang, Y. Acetone sensing performances based on nanoporous TiO_2synthesized by a facile hydrothermal method. *Sens. Actuators B Chem.* **2017**, *238*, 491–500. [CrossRef]
39. Alev, O.; Şennik, E.; Öztürk, Z.Z. Improved gas sensing performance of p-copper oxide thin film/n-TiO_2 nanotubes heterostructure. *J. Alloys Compd.* **2018**, *749*, 221–228. [CrossRef]
40. Sun, T.; Wang, M. A comparative study on titania layers formed on Ti, Ti-6Al-4V and NiTi shape memory alloy through a low temperature oxidation process. *Surf. Coatings Technol.* **2010**, *205*, 92–101. [CrossRef]
41. Wu, J.M.; Zhang, T.W.; Zeng, Y.W.; Hayakawa, S.; Tsuru, K.; Osaka, A. Large-scale preparation of ordered titania nanorods with enhanced photocatalytic activity. *Langmuir* **2005**, *21*, 6995–7002. [CrossRef] [PubMed]
42. Yamabi, S.; Imai, H. Crystal phase control for titanium dioxide films by direct deposition in aqueous solutions. *Chem. Mater.* **2002**, *14*, 609–614. [CrossRef]
43. Barsan, N.; Weimar, U. Conduction Model of Metal Oxide Gas Sensors. *J. Electroceramics* **2001**, *7*, 143–167. [CrossRef]
44. Gu, H.; Wang, Z.; Hu, Y. Hydrogen gas sensors based on semiconductor oxide nanostructures. *Sensors* **2012**, *12*, 5517–5550. [CrossRef]
45. Simon, Q.; Barreca, D.; Gasparotto, A.; MacCato, C.; Tondello, E.; Sada, C.; Comini, E.; Sberveglieri, G.; Banerjee, M.; Xu, K.; et al. CuO/ZnO nanocomposite gas sensors developed by a plasma-assisted route. *ChemPhysChem* **2012**, *13*, 2342–2348. [CrossRef]
46. Barreca, D.; Carraro, G.; Comini, E.; Gasparotto, A.; Maccato, C.; Sada, C.; Sberveglieri, G.; Tondello, E. Novel Synthesis and Gas Sensing Performances of CuO–TiO_2 Nanocomposites Functionalized with Au Nanoparticles. *J. Phys. Chem. C* **2011**, *115*, 10510–10517. [CrossRef]

47. Zhuang, J.; Rusu, C.N.; Yates, J.T. Adsorption and Photooxidation of CH_3 CN on TiO_2. *J. Phys. Chem. B* **1999**, *103*, 6957–6967. [CrossRef]
48. Lee, M.J.; Cheong, H.W.; Son, L.D.N.; Yoon, Y.S. Surface reaction mechanism of acetonitrile on doped SnO_2 sensor element and its response behavior. *Jpn. J. Appl. Phys.* **2008**, *47*, 2119–2121. [CrossRef]
49. Dutta, P.K.; Ginwalla, A.; Hogg, B.; Patton, B.R.; Chwieroth, B.; Liang, Z.; Gouma, P.; Mills, M.; Akbar, S. Interaction of Carbon Monoxide with Anatase Surfaces at High Temperatures: Optimization of a Carbon Monoxide Sensor. *J. Phys. Chem. B* **1999**, *103*, 4412–4422. [CrossRef]
50. Savage, N.O.; Akbar, S.A.; Dutta, P.K. Titanium dioxide based high temperature carbon monoxide selective sensor. *Sens. Actuators B Chem.* **2001**, *72*, 239–248. [CrossRef]
51. Bârsan, N.; Ionescu, R. The mechanism of the interaction between CO and an SnO_2 surface: The role of water vapour. *Sens. Actuators B Chem.* **1993**, *12*, 71–75. [CrossRef]
52. Moon, J.; Hedman, H.P.; Kemell, M.; Suominen, A.; Mäkilä, E.; Kim, H.; Tuominen, A.; Punkkinen, R. A study of monitoring hydrogen using mesoporous TiO_2 synthesized by anodization. *Sens. Actuators B Chem.* **2013**, *189*, 246–250. [CrossRef]
53. Bhowmik, B.; Bhattacharyya, P. Highly stable low temperature alcohol sensor based on hydrothermally grown tetragonal titania nanorods. *RSC Adv.* **2015**, *5*, 82159–82168. [CrossRef]
54. Shastri, A.G.; Schwank, J. Adsorption-induced conductance changes of thin Pt films and PtPd/TiO_2 gas sensors. *Appl. Surf. Sci.* **1987**, *29*, 341–360. [CrossRef]
55. Roland, U.; Salzer, R.; Braunschweig, T.; Roessner, F.; Winkler, H. Investigations on hydrogen spillover. Part 1.—Electrical conductivity studies on titanium dioxide. *J. Chem. Soc. Faraday Trans.* **1995**, *91*, 1091–1095. [CrossRef]
56. Ruiz, A.; Dezanneau, G.; Arbiol, J.; Cornet, A.; Morante, J. Study of the influence of Nb content and sintering temperature on TiO_2 sensing films. *Thin Solid Films* **2003**, *436*, 90–94. [CrossRef]
57. Jinkawa, T.; Sakai, G.; Tamaki, J.; Miura, N.; Yamazoe, N. Relationship between ethanol gas sensitivity and surface catalytic property of tin oxide sensors modified with acidic or basic oxides. *J. Mol. Catal. A Chem.* **2000**, *155*, 193–200. [CrossRef]
58. Comini, E.; Faglia, G.; Sberveglieri, G.; Calestani, D.; Zanotti, L.; Zha, M. Tin oxide nanobelts electrical and sensing properties. *Sens. Actuators B Chem.* **2005**, *111–112*, 2–6. [CrossRef]
59. Sadek, A.Z.; Partridge, J.G.; McCulloch, D.G.; Li, Y.X.; Yu, X.F.; Wlodarski, W.; Kalantar-zadeh, K. Nanoporous TiO_2thin film based conductometric H_2 sensor. *Thin Solid Films* **2009**, *518*, 1294–1298. [CrossRef]
60. Sennik, E.; Kilinc, N.; Ozturk, Z.Z. Electrical and VOC sensing properties of anatase and rutile TiO_2 nanotubes. *J. Alloys Compd.* **2014**, *616*, 89–96. [CrossRef]
61. Park, S.; An, S.; Ko, H.; Lee, S.; Kim, H.W.; Lee, C. Enhanced ethanol sensing properties of TiO_2/ZnO core-shell nanorod sensors. *Appl. Phys. A Mater. Sci. Process.* **2014**, *115*, 1223–1229. [CrossRef]
62. Xia, X.; Wu, W.; Wang, Z.; Bao, Y.; Huang, Z.; Gao, Y. A hydrogen sensor based on orientation aligned TiO_2thin films with low concentration detecting limit and short response time. *Sens. Actuators B Chem.* **2016**, *234*, 192–200. [CrossRef]
63. *Acute Exposure Guideline Levels for Selected Airborne Chemicals*; National Academies Press: Washington, DC, USA, 2016; Volume 16, ISBN 9780309300964.